Article:
Aungwerojwit, A., Gänsicke, B.T., Breedt, E. et al. (2025) Follow-up on three poorly studied AM CVn stars. Monthly Notices of the Royal Astronomical Society, 537 (4). pp. 3078-3090. ISSN: 0035-8711

https://doi.org/10.1093/mnras/staf173

Monthly Notices of the ROYAL ASTRONOMICAL SOCIETY

MNRAS **537,** 3078–3090 (2025) https://doi.org/10.1093/mnras/staf173
Advance Access publication 2025 January 29

Follow-up on three poorly studied AM CVn stars

Amornrat Aungwerojwit [1], Boris T. Gänsicke [2]★ E. Breedt [3], S. Arjyotha,[1]† J. J. Hermes [4], F.-J. Hambsch,[5,6,7] A. Kumar,[2,8] S. H. Ramírez [2], T. G. Wilson [2], V. S. Dhillon [9,10] T. R. Marsh [2]† S. Poshyachinda,[11] S. Scaringi,[12,13] J. B. Haislip[14] and D. E. Reichart[14]

[1]*Department of Physics, Faculty of Science, Naresuan University, Phitsanulok 65000, Thailand*
[2]*Department of Physics, University of Warwick, Coventry CV4 7AL, UK*
[3]*Institute of Astronomy, University of Cambridge, Cambridge CB3 0HA, UK*
[4]*Department of Astronomy, Boston University, 725 Commonwealth Avenue, Boston, MA 02215, USA*
[5]*Vereniging Voor Sterrenkunde (VVS), Oostmeers 122 C, B-8000 Brugge, Belgium*
[6]*Bundesdeutsche Arbeitsgemeinschaft für Veränderliche Sterne, Munsterdamm 90, D-12169 Berlin, Germany*
[7]*AAVSO, 185 Alewife Brook Parkway, Suite 410, Cambridge, MA 02138, USA*
[8]*Department of Physics, Royal Holloway, University of London, Egham Hill, Surrey TW20 0EX, UK*
[9]*Department of Physics and Astronomy, University of Sheffield, Sheffield S3 7RH, UK*
[10]*Instituto de Astrofísica de Canarias, E-38205 La Laguna, Tenerife, Spain*
[11]*National Astronomical Research Institute of Thailand (Public Organization), Chiangmai 50180, Thailand*
[12]*Centre for Extragalactic Astronomy, Department of Physics, University of Durham, South Road, Durham DH1 3LE, UK*
[13]*INAF – Osservatorio Astronomico di Capodimonte, Salita Moiariello 16, I-80131 Naples, Italy*
[14]*Department of Physics and Astronomy, University of North Carolina at Chapel Hill, Chapel Hill, NC 27599, USA*

Accepted 2025 January 24. Received 2025 January 23; in original form 2024 November 25

ABSTRACT

We report follow-up observations of three poorly studied AM CVn-type binaries: CRTS CSS150211 J091017−200813, NSV 1440, and SDSS J183131.63+420220.2. Analysing time-series photometry obtained with a range of ground-based facilities as well as with the *Transiting Exoplanet Survey Satellite* (*TESS*), we determine the superhump period of CRTS J0910−2008 as $P_{\rm sh} = 29.700 \pm 0.004$ min and the orbital period of NSV 1440 as $P_{\rm orb} = 36.56 \pm 0.03$ min. We also confirm a photometric period of $P = 23.026 \pm 0.097$ min in SDSS J1831+4202, which is most likely the superhump period. We also report the first optical spectroscopy of CRTS J0910−2008 and NSV 1440 which unambiguously confirms both as AM CVn systems. We briefly discuss the distribution in the Hertzsprung–Russell diagram of the currently known sample of 63 AM CVn stars with known periods and *Gaia* data.

Key words: binaries: close – stars: dwarf novae – stars: individual: CRTS J091017.43−200812.3, NSV 1440, SDSS J183131.63+420220.2 – novae, cataclysmic variables.

1 INTRODUCTION

AM CVn-type stars are short-period ($P_{\rm orb} \simeq 5$–68 min), helium-dominated binaries in which a white dwarf accretes material from a close companion through Roche lobe overflow. Their compact configuration implies that the companion itself must be an evolved star, likely another white dwarf or a semi-degenerate helium star. They are expected to be bright sources of low-frequency gravitational waves (Nelemans, Yungelson & Portegies Zwart 2004; Amaro-Seoane et al. 2012) and hence some of the first sources to be detected by the *LISA* Gravitational Wave Observatory (Korol et al. 2017; Kupfer et al. 2018). AM CVn stars may also be the sources of helium novae (Kato et al. 2008; Woudt et al. 2009), Type Ia supernovae (Shen & Bildsten 2014), and the sub-luminous '.Ia' explosions (Bildsten et al. 2007). For a detailed review and a summary of the known population's properties, see Solheim (2010) and Ramsay et al. (2018), respectively.

In all but the most compact of these binaries (Marsh, Nelemans & Steeghs 2004), accretion occurs via an accretion disc. Just as is the case in the hydrogen-dominated cataclysmic variables (CVs) (Osaki 1974), the helium discs of AM CVn stars are subject to a thermal instability which can cause quasi-regular outbursts of several magnitudes (Kotko et al. 2012; Ramsay et al. 2012). As a result, AM CVn systems are detected as transients in large-area photometric surveys including the Catalina Real-time Transient Survey (CRTS; Drake et al. 2009), the All-Sky Automated Survey for Supernovae (ASAS-SN; Shappee et al. 2014; Kochanek et al. 2017), Zwicky Transient Facility (ZTF; Bellm et al. 2019; Masci et al. 2019), and the Gravitational-wave Optical Transient Observer (GOTO; Steeghs et al. 2022). The dwarf nova outbursts of AM CVn are generally not distinguishable from those of the more common hydrogen CVs, and additional follow-up is usually required to confirm the AM CVn nature (Levitan et al. 2011; van Roestel et al. 2021; Khalil et al. 2024).

★ E-mail: boris.gaensicke@gmail.com
† Deceased.

Table 1. Basic properties of the three AM CVn stars analysed in this paper.

Object	RA (IRCS 2000)	Dec. (IRCS 2000)	*Gaia* DR3 source_id	Parallax (mas)	Typical magnitude (mag)
CRTS CSS150211 J091017−200813	09:10:17.45	−20:08:12.5	5679545150277507328	1.35 ± 0.14	$G = 19.4$
NSV 1440	03:55:17.97	−82:26:11.3	4616023664815517440	3.08 ± 0.08	$G = 18.5$
SDSS J183131.63+420220.2	18:31:31.63	+42:02:20.2	2111270721441518208	0.71 ± 0.07	$G = 17.5$

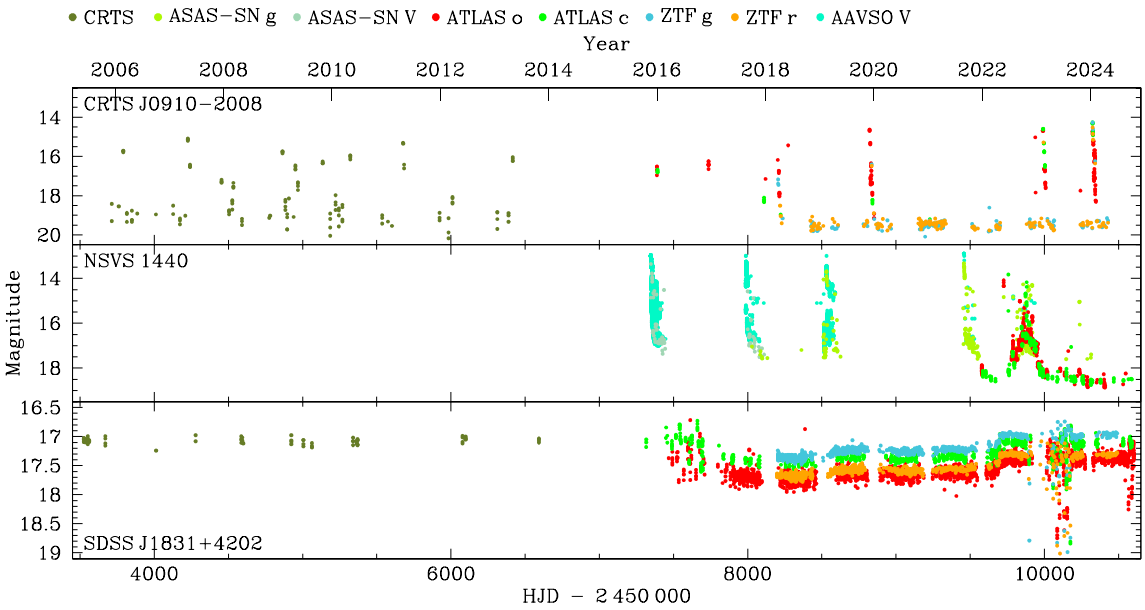

Figure 1. Long-term archival light curves of the three AM CVn stars discussed in this paper. CRTS J0910−2008 and NSV 1440 display frequent outbursts. SDSS J1831+4202 spends most of the time in a stable high state with some changes in its long-term brightness, but undergoes a short phase during which the accretion disc becomes thermally unstable (HJD $\simeq$ 2 457 500 and HJD $\simeq$ 2 460 000).

AM CVn stars with $P_{\rm orb} \lesssim 18$ min have stable, hot accretion discs and do not display outbursts and systems with $P_{\rm orb} \gtrsim 45$ min have such low-mass transfer rate that they rarely outburst (e.g. Levitan et al. 2015, even though the outburst properties are somewhat more complex, see Duffy et al. 2021). Discovering these systems is more difficult and requires either the detection of eclipses (van Roestel et al. 2022), orbital variability (Smak 1967), spectra dominated by helium lines (Greenstein & Matthews 1957; Carter et al. 2013), or X-ray emission (Rodriguez et al. 2023). The serendipitous discovery of bright ($G \simeq 14.3$) short-period ($P_{\rm orb} \simeq 23$ min) AM CVn systems from *TESS* photometry demonstrates that the current census of AM CVn systems is still strongly biased and incomplete (Green et al. 2024).

As AM CVn systems are both less common and intrinsically less luminous (because of their smaller accretion discs) than hydrogen-rich CVs, the majority of the known systems are faint: Green (2023) maintains a catalogue of AM CVn stars,[1] and the median apparent magnitude of the 107 confirmed systems is $G \simeq 19.5$. Consequently, a detailed characterization of this population is challenging, in particular orbital phase-resolved spectroscopy, even with large-aperture telescopes. Fortunately, the orbital period of AM CVn stars can often be estimated photometrically from a phenomenon known as superhumps, a dynamical interaction of the outer edge of the accretion disc with the companion star (Whitehurst & King 1991) resulting in brightness variations on a period with a few per cent longer than the orbital one (Patterson et al. 2005; Kato et al. 2009).

Here, we report time-series photometry of three AM CVn candidates obtained using a variety of small to medium-size telescopes (0.4–2.4 m). Sections 3 and 4 describe our follow-up observation and analysis of the data. We discuss the three new binaries in the context of the known population in Section 5.

2 THE THREE AM CVN SYSTEMS

2.1 CRTS CSS150211 J091017−200813

We obtained the first observations of CRTS CSS150211 J091017−200813 (hereafter CRTS J0910−2008, see Table 1) in response to an outburst detected by the Catalina Sky Survey (CSS) telescope of CRTS on 2015 February 11 (Drake et al. 2009). The system, typically at $V \simeq 19.5$ mag in quiescence, was detected at $V = 16.1$ during this outburst. This is the only outburst of this system observed by CSS, but upon querying the CRTS archive, we discovered that the CRTS Siding Springs Survey (SSS) telescope observed many previous outbursts of this system, the brightest of which was measured to be $V = 15.08$. The full CRTS light curve covered more than 12 yr is shown in Fig. 1. We detected

[1] https://zenodo.org/records/12672892

another outburst of this object on 2018 March 18, while observing it using the 2.4-m Thai National Telescope (TNT). The object reached $KG5 \simeq 14.0$ during our observations,[2] but it was not observed during this time by the transient surveys.

2.2 ASASSN-15sz/NSV 1440

The ASAS-SN survey alerted on a potential CV, ASASSN-15sz (see Table 1), on 2015 November 20. The discovery outburst reached $V = 12.84$ (Fig. 1), but the target is below the ASAS-SN detection limit ($V \lesssim 17$) in quiescence. It was however detected by *Gaia* at $G = 18.52$ (DR1; Gaia Collaboration 2018). The International Variable Star index (Watson, Henden & Price 2006) revealed that the object had previously been identified as a variable star, although its nature was not determined at the time. The name originally assigned to the variable, NSV 1440,[3] has been widely adopted for this star, and we follow that convention here. The 2015 outburst, as well as another in 2017, was studied in detail by Isogai et al. (2019). They showed that NSV 1440 was the first AM CVn system to display the double superoutburst characteristic that is normally seen in hydrogen dwarf novae of WZ Sge-type.[4]

2.3 SDSS J183131.63+420220.2

SDSS J183131.63+420220.2 (hereafter SDSS J1831+4202, see Table 1) was identified by Inight et al. (2023) as an AM CVn star based on its SDSS spectrum displaying a blue continuum with broad He I absorption lines and long-term variability in its ZTF light curve. Kato (2023) detected a photometric 23 min signal within the ZTF data, and suggested that this could be the orbital period of the system. We included this system in our survey to confirm the photometric period.

3 OBSERVATIONS

3.1 Time-series photometry

Our follow-up photometry was carried out at the Cerro Tololo Inter-American Observatory in Chile, using the 0.6 m Panchromatic Robotic Optical Monitoring and Polarimetry Telescopes (PROMPT8), at the Thai National Observatory (TNO) on Doi Inthanon, Thailand, using the 2.4-m TNT as well as the 0.5-m-TNO telescopes, and at the 0.4-m telescope of the Remote Observatory Atacama Desert (ROAD), San Pedro, Chile. PROMPT8 and the TNO are both operated by the National Astronomical Research Institute of Thailand (NARIT). ROAD is a privately owned telescope hosted at SPACEOBS.[5] A full log of the observations is presented in Tables A1–A4.

3.1.1 CRTS J0910−2008

CSS detected an ≈ 3.4 mag outburst of CRTS J0910−2008 on 2015 February 11 and reported it to their transients wbpage. We immediately started taking time-series photometry on PROMPT8, observing the target during the period 2015 February 12–27 whenever the weather allowed, for approximately 4–8 h per night. The PROMPT8 telescope is equipped with a 2 k × 2 k Apogee CCD with a pixel scale of 0.70 arcsec pixel^{-1}, providing a 23.8 arcmin × 23.8 arcmin field of view. The images were taken in V filter in unbinned mode. The raw images were bias-subtracted, dark current-subtracted, and flat-fielded using the SKYNET automated reduction pipeline. We extracted aperture photometry using SEXTRACTOR (Bertin & Arnouts 1996) and converted the instrumental magnitudes to apparent magnitudes using the comparison stars listed in Table A2.

Additional observations were carried out with the TNT from 2018 to 2024, the data were reduced using the ULTRACAM reduction pipeline, described in Dhillon et al. (2007). We detected another outburst on 2018 March 18 at a brightness of $KG5 = 14.0$. A full log of the observations is presented in Table A2.

3.1.2 NSV 1440

We used PROMPT8 to obtain time-series photometry of the system during 2015 November 22–27. The images were taken in V filter on the first three nights while the object was bright ($V = 12.4$–12.6), and filter-less on the next two nights when the object had dropped to a faint state at $\simeq 18$ mag. The data were reduced and extracted in the same manner as for CRTS J0910−2008 described above.

Fig. 1 shows that ASAS-SN detected several additional bright outbursts of this object. In this paper, we present our own observations of the 2015 outburst which were not included in Isogai et al. (2019), as well as an analysis of the 2019 outburst, which was observed with the ROAD 0.4-m telescope for 68 d. A log of the observations is given in Table A3.

3.1.3 SDSS J1831+4202

We obtained time-series photometry of SDSS J1831+4202 using ULTRASPEC (Dhillon et al. 2014) at the TNT. All images were taken using the $KG5$ filter with 2 × 2 binning mode. The data were reduced using HiPERCAM data reduction pipeline.[6] A superhump-like structure was detected on 2023 May 3 when the object was at 17.1 mag. The detailed log of the observations is given in Table A4.

3.2 Identification spectroscopy

CRTS J0910−2008 and NSV 1440 were identified as AM CVn candidates because of their short-period photometric variability (Section 4), and we obtained identification spectroscopy to confirm this classification.

We obtained an optical spectrum of CRTS J0910−2008 at the European Southern Observatory's Very Large Telescope on 2015 May 5, using the FORS2 spectrograph. The spectrum shown in Fig. 2 is the average of four 600 s exposures, two taken using the GRIS_300V+10 grism and two using the GRIS_300I+11 grism. The combined spectrum covers the range 3830–10 110 Å at 12 Å resolution. Conditions were clear at the time of the observation, but morning twilight was too cloudy to take a standard star spectrum, so we derived an approximate flux calibration using an archival observation of the standard star LTT3864, taken with the same instrumental set-up.

For NSV 1440, we obtained low-resolution optical spectra using a 930 line mm^{-1} grating with the Goodman spectrograph on the

[2]The $KG5$ filter is a broad filter which includes most of the SDSS u', g', and r' bandpasses. See Hardy et al. (2017) for the transmission curve and further details.
[3]At the time of publishing, Simbad reports the wrong object for NSV 1440.
[4]WZ Sge stars are evolved hydrogen CVs with large amplitude, but infrequent, outbursts. See Kato (2015) for a detailed review.
[5]San Pedro de Atacama Celestial Explorations
[6]https://github.com/HiPERCAM/hipercam

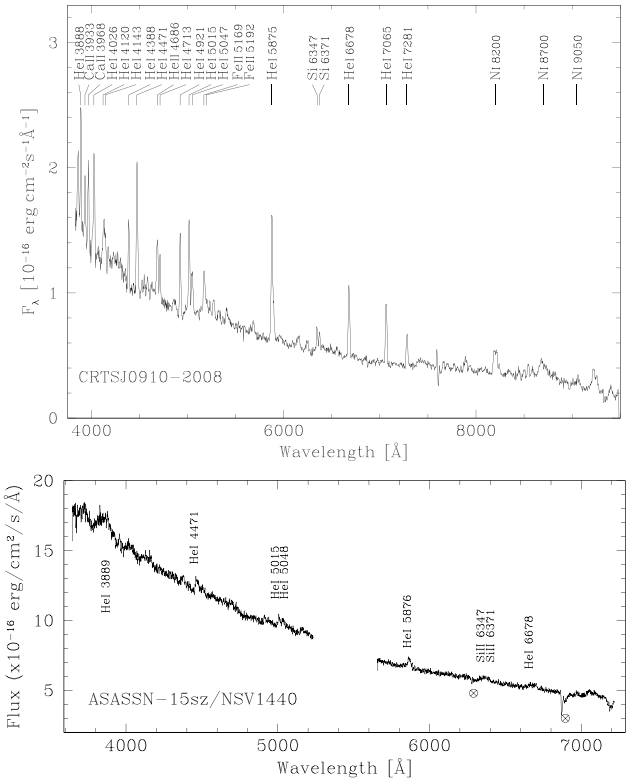

Figure 2. Identification spectra of CRTS J0910–2008 (top) and NSV 1440 (bottom). The strongest emission lines are labelled, as well as oxygen absorption from the earth's atmosphere (crossed circle symbols).

4.1-m SOAR telescope (Clemens, Crain & Anderson 2004) on the night of 2016 January 8. Using two different grating and camera angles, we obtained set-ups that cover the wavelength range 3600–5200 Å (4 × 300 s exposures) and 5640–7200 Å (4 × 300 s exposures), with a dispersion of roughly 0.84 Å pixel^{-1}. We used a 3.2 arcsec slit, so our spectral resolution is seeing limited, roughly 4 Å in the mean 1.3 arcsec seeing during our observations. We flux calibrated our spectra using the spectro-photometric standard GD 108.

The reduction of all spectra and calibration frames were done using standard STARLINK routines (Currie et al. 2014) and then the spectra were optimally extracted using the STARLINK package PAMELA (Marsh 1989). The wavelength and flux calibration, as well as a heliocentric correction to the time stamps, were applied using MOLLY.[7]

The spectrum of CRTS J0910−2008 is dominated by strong helium emission, along with emission lines from He, Ca, Si, N, and Fe, as shown in Fig. 2. The feature at 7600 Å is residual telluric absorption. No lines from hydrogen are detected in the spectrum, consistent with those of other AM CVn stars.

The emission features are weaker in NSV 1440, but we detect lines of He, Si and Ca in this spectrum as well (Fig. 2). No feature from H is detected. This confirms the classification of NSV 1440 as an AM CVn star.

[7]MOLLY was written by T. R. Marsh and is available from http://www.warwick.ac.uk/go/trmarsh/software/.

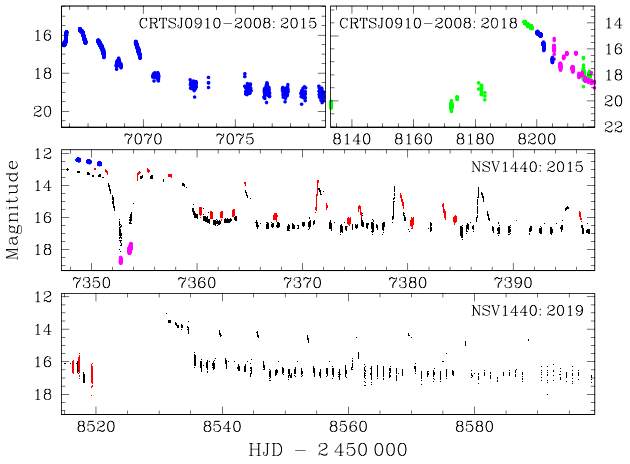

Figure 3. Top panels: Our complete light-curve data of the 2015 and 2018 outbursts of CRTS J0910−2008 obtained in *V* (blue), *KG*5 (green), and clear (magenta) filters. Bottom two panels: The 2015 and 2019 AAVSO light curves of NSV 1440 with *V*- and *R*-band data shown in black and red, respectively. Overlayed is our data in the *V* (blue) and clear filter photometry (magenta).

4 ANALYSIS

4.1 CRTS J0910−2008

We observed CRTS J0910−2008 in outburst twice. Our observations covered a period of 13 d in 2015 February and 27 d in 2018 March. The complete light curves for the two outbursts are shown in Fig. 3.

4.1.1 2015 outburst

We obtained 4 h of time-series photometry on February 12, which showed that the object was on the rise to outburst, brightening by ≃ 0.4 mag towards the end of the night (Fig. 5). A short-time-scale variation of ≃ 30 min was also visible, suggesting the object might be a system below the conventional period minimum of CVs. In order to confirm the nature of the object, we continued our observations for as long as possible. The light curves on February 13–14 covered ≃ 7.5 h each night, and both presented the same trend of declining brightness (∼ 0.7–0.9 mag) plus a consistent signal of short-time-scale modulation of ≃ 30 min as seen on the first night (Fig. 5). On February 15, the object dropped in brightness by nearly one magnitude, but it re-brightened again on the next night, with a light curve very similar to those of February 13–14. Overall the light curves of CRTS J0910−2008 on February 12–16 can be described as a ≃ 0.1 mag, ≃ 30 min quasi-periodic modulation with a 'superhump-like' structure, superimposed on a trend of ∼ 0.5–1.0 mag night-to-night variation. The superhump structure, however, disappeared on February 17 when the object dropped to ≃ 18.1 mag. A short-time-scale variation of ≃ 15 min can be noticed in the light curve on this night. For February 19–27, the object remained in a faint state of ≥ 18 mag, which reaches telescope limit. We obtained five images of 100 s each every 20 min to monitor the evolution of the outburst; however, these light curves were too short to confirm ≃ 15 min signal. The two-week light curve shown in the top panel of Fig. 3 shows that the object returned to its quiescent state within a week after the outburst was detected by CSS.

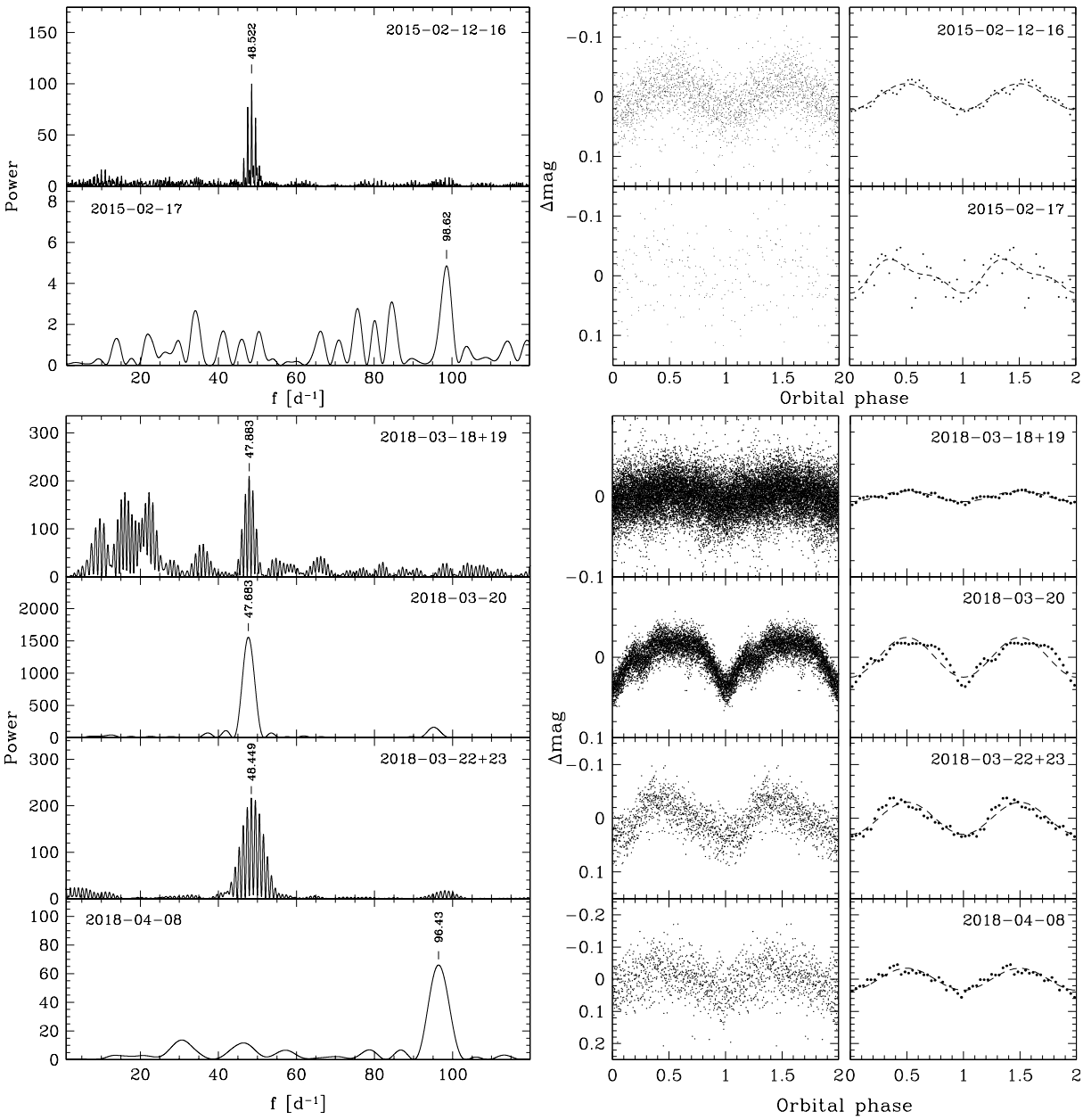

Figure 4. Lomb–Scargle periodograms (left panels) and phase-folded light curves (right two panels, actual data and binned into 30 phases) of CRTS J0910−2008 during the 2015 outburst (top two panels) and the 2018 outburst (bottom four panels). The dates or date ranges of the data used for the individual analyses are indicated near the top of each panel. Most of the data show a strong signal at $f \simeq 48\,\mathrm{d}^{-1}$, which we interpret as the superhump period of the system, $P_{\rm sh} \simeq 30$ min. On two occasions (2015 February 17 and 2018 April 8) we detected a signal at $f \simeq 97\,\mathrm{d}^{-1}$ which we interpret as the second harmonic of the superhump.

The superhump periods measured on the individual nights from February 12–16 were very similar, so we combined the data from these five nights. We detrended the light curves for the overall variations in the average brightness of the system and then computed a Scargle (1982) periodogram using the `MIDAS/TSA` context. The strongest signal is found at $f = 48.522 \pm 0.007\,\mathrm{d}^{-1}$ where the error is determined from fitting a sine wave to the data. We identified this signal as a superhump period $P_{\rm sh} = 29.677 \pm 0.004$ min (Fig. 4, top left panel). The phase-folded light curve (Fig. 4, right panels) has a quasi-sinusoidal morphology also seen in the individual light curves.

In addition, we also computed a Scargle periodogram of the February 17 light curve, after detrending the low-frequency variation (Fig. 4, second-left panel). It reveals a weak signal at $f = 98.62 \pm 0.65\,\mathrm{d}^{-1}$ or $P = 14.6 \pm 0.1$ min. This is nearly double the peak frequency of the nights before, likely a harmonic of the superhump signal.

4.1.2 2018 outburst

In 2018 January to March, we obtained TNT time-series photometry of CRTS J0910−2008 in its quiescent state ($\sim$ 19.0–20.4 mag) to

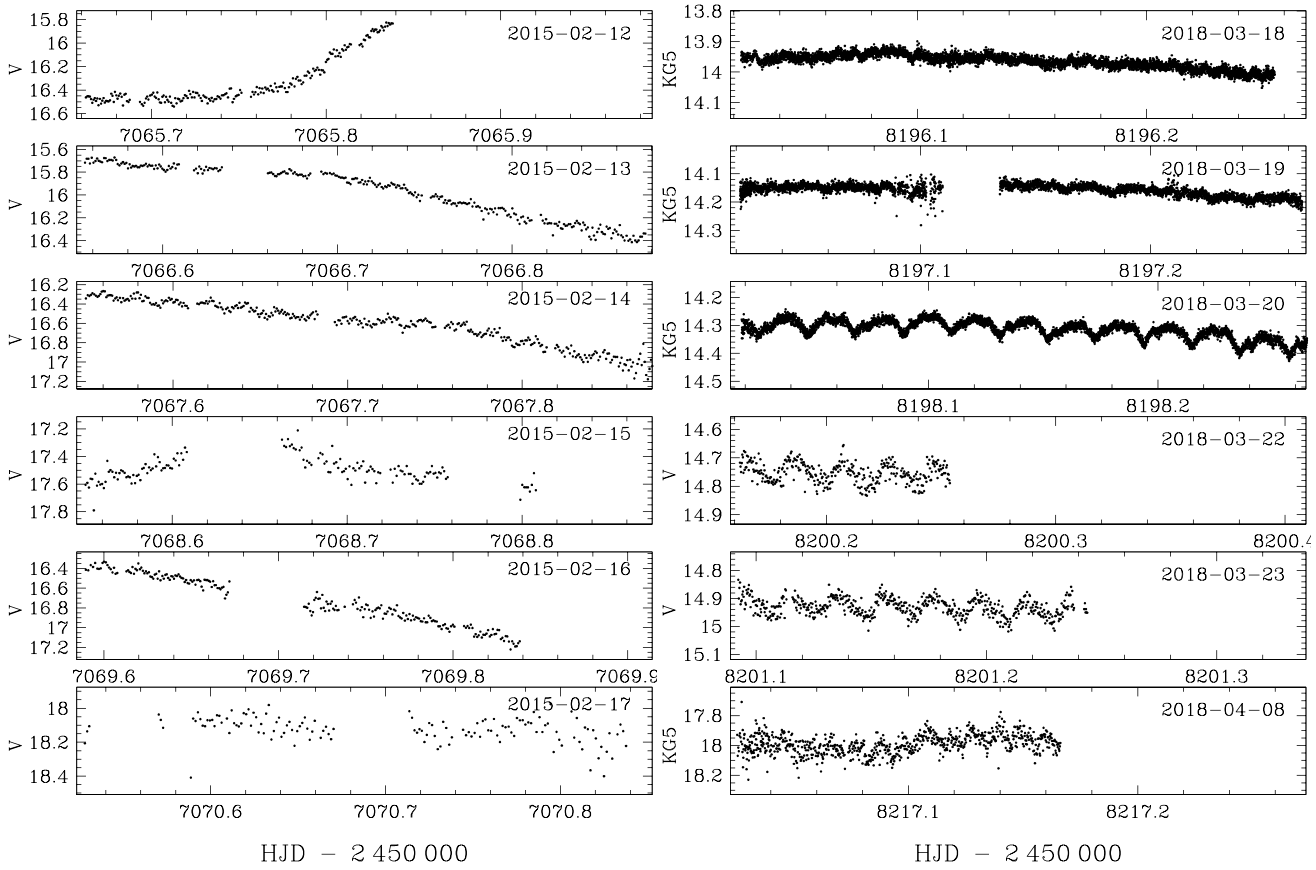

Figure 5. Light curves of CRTS J0910−2008 during the 2015 and 2018 outbursts used for superhump-period analysis. *Left:* 2015 outburst. The light curves obtained on 12–14 February are dominated by a $\simeq 15$ min modulation superimposed on the declining night-to-night trend in the brightness of the system as it declines from the outburst. The system briefly re-brightened on February 16 (see Fig. 1) before fading into quiescence. *Right:* During the 2018 outburst, we detected superhump variability throughout many subsequent nights.

probe for variability (see Table A2). Overall the light curves of CRTS J0910−2008 during quiescence display small variations of ~ 0.4–0.6 mag. A Scargle periodogram of the $\simeq 6$ h quiescent data suggests a possible periodicity at ~ 32.9 min, but there are many alias signals so additional photometry is necessary to confirm this periodicity. On March 18, we detected CRTS J0910−2008 in outburst again. It had a mean magnitude of ~ 14.0, which is brighter than the mean magnitudes of ~ 15.0–16.0 of the previous outbursts detected by CSS and SSS. We followed the outburst over a total of 21 nights with a variety of telescopes, as weather and telescope access allowed (Table A2). We show examples of the superhump variability detected during the period of March 18 and April 8 in Fig. 5.

A weak short-period variability of $\simeq 30$ min appeared in the March 18 and 19 data and it grew to a clearly visible superhump signal in the March 20 light curve. This superhump signal dominated the light curves of March 22–23 as the object brightness declined to $V = 14.8$–14.9. On March 24, the object's brightness dropped by one magnitude and the superhump was less obvious in our $\simeq 1$ h long light curve, we therefore did not include that night in the analysis. In April, we detected the system at $\simeq 18.0$ mag. The light curve on April 8 reveals a short-time-scale variation of $\simeq 15$ min as found in the 2015 outburst. This short-time-scale brightness variation is shown in the bottom panel of Fig. 5.

In order to study the evolution of the superhump during the 2018 outburst, we created Scargle periodograms for several subsets of data, depending on morphology of the light curves (Fig. 4). As before, we removed the low-frequency trends in the light curves before calculating the periodograms. The March 18 and 19 light curves display low amplitude, short-period variations and their Scargle periodogram confirms this, with a peak at $f = 47.883 \pm 0.015\,\mathrm{d}^{-1}$, or 30.073 ± 0.009 min. By March 20, the amplitude of the variations had grown to 0.1 mag and the Scargle periodogram indicated a slightly longer period of $P = 30.199 \pm 0.016$ min, or $f = 47.683 \pm 0.025\,\mathrm{d}^{-1}$. The combined light curves from March 22 and 23 gave a peak in the Scargle periodogram at $f = 48.449 \pm 0.012\,\mathrm{d}^{-1}$, or $P_{\rm sh} = 29.722 \pm 0.007$ min consistent with the superhump period from the 2015 outburst. We take the average of the two values as the superhump period of CRTS J0910−2008, $P_{\rm sh} = 29.700 \pm 0.004$ (see Table A5 for a summary). Finally, the Scargle periodogram of the April 8 data has a peak at $f = 96.43 \pm 0.30\,\mathrm{d}^{-1}$, or $P = 14.93 \pm 0.05$ min.

4.2 NSV 1440

4.2.1 2015 outburst

We obtained time-series photometry of NSV 1440 during 2015 November 22–27. The full light curve is shown in Fig. 3. On November 22–24, the object was in very bright state, $V = 12.4$–12.6, and then faded rapidly to 18.7 mag on November 26, but rose again

in brightness the next night. Poor weather on November 25 prevented us from taking any observations on that night.

Our observations on November 22–24 revealed small amplitude variations ($\simeq 0.02$ mag, Fig. 6, top panel) with a period of 18.168 ± 0.003 min ($f = 79.260 \pm 0.014\,\mathrm{d}^{-1}$) for the combined data set (Fig. 6, middle panel). Treating the nights individually yields periods close to this value, that agree with each other within the error bars. We interpret this signal as the harmonic of the superhump period, i.e. 36.336 ± 0.003 min. This value is almost identical to the early superhump period reported by Isogai et al. (2019).

The light curve on November 27 reveals a prominent superhump structure while the system was brightening overall by $\simeq 0.3$ mag (Fig. 6, second-top panel). The Lomb–Scargle periodogram from these data shows a strong signal at $f = 38.37 \pm 0.13\,\mathrm{d}^{-1}$ (Fig. 6, middle panel) which we define as the superhump period $P_{\mathrm{sh}} = 37.53 \pm 0.13$ min, longer than the period of the 'stage A' superhumps (36.98 min) reported by Isogai et al. (2019). The corresponding phase-folded light curves of these two frequencies are illustrated in Fig. 6 (bottom panels).

4.2.2 *2019 outburst*

We started time-series observations immediately following the detection of another bright outburst of NSV 1440 on 2019 February 16 (Stubbings 2019, vsnet-alert 23005). The system stayed bright ($V < 14$) for four nights before fading back to $V \simeq 16$. Over the course of a further 64 nights, we observed six rebrightenings, as well as one small ($\simeq 1$ mag) outburst (Fig. 3), similar to the behaviour seen in the 2015 and 2017 outbursts (Isogai et al. 2019). A periodogram computed from the observations obtained during the first 4 d of the outburst shows a strong signal at $\simeq 39.46\,\mathrm{d}^{-1}$, corresponding to $P = 36.525 \pm 0.017$ min, similar to that of the 'stage B' superhumps reported by Isogai et al. (2019).

4.2.3 TESS *observations and the 2022 'high state'*

The *TESS* mission observed NSV 1440 in short-cadence mode (120 s exposures) during sectors 27, 28, 39, and 65–68. The first three sectors were obtained during quiescence, and the last four sectors were obtained following a 'high state' where NSV 1440 was about two magnitudes brightener than its typical quiescent level (Fig. 7). During that state, NSV 1440 exhibited multiple short outbursts with amplitudes of $\simeq 2$ mag above the baseline brightness.

Extremely long brightening events have been observed in a number of other AM CVn stars including SDSS J080710.33+485259.6 ($P_{\mathrm{orb}} \simeq 53$ min; Rivera Sandoval, Maccarone & Pichardo Marcano 2020), SDSS J113732.34+405458.0 ($P_{\mathrm{orb}} \simeq 60$ min; Rivera Sandoval et al. 2021), and ASASSN-21au ($P_{\mathrm{orb}} \simeq 58$ min; Rivera Sandoval et al. 2022). All three systems have much longer periods than NSV 1440, and the detailed morphology of their brightening events differs from that seen in NSV 1440, having a slow rise followed by a fairly sudden fading, and a re-brightening event in the case of ASASSN-21au. The fact that NSV 1440 exhibits normal outbursts throughout the bright state indicates that at least large parts of the disc continue to undergo thermal instabilities. The nature of the brightenings has been discussed in the context of episodes of enhanced mass transfer as well as thermal instabilities within the disc (Rivera Sandoval et al. 2022, and Kato & Stubbings (2023) for the case of NSV 1440). However, no consensus has yet been reached on the exact physical origin of these events.

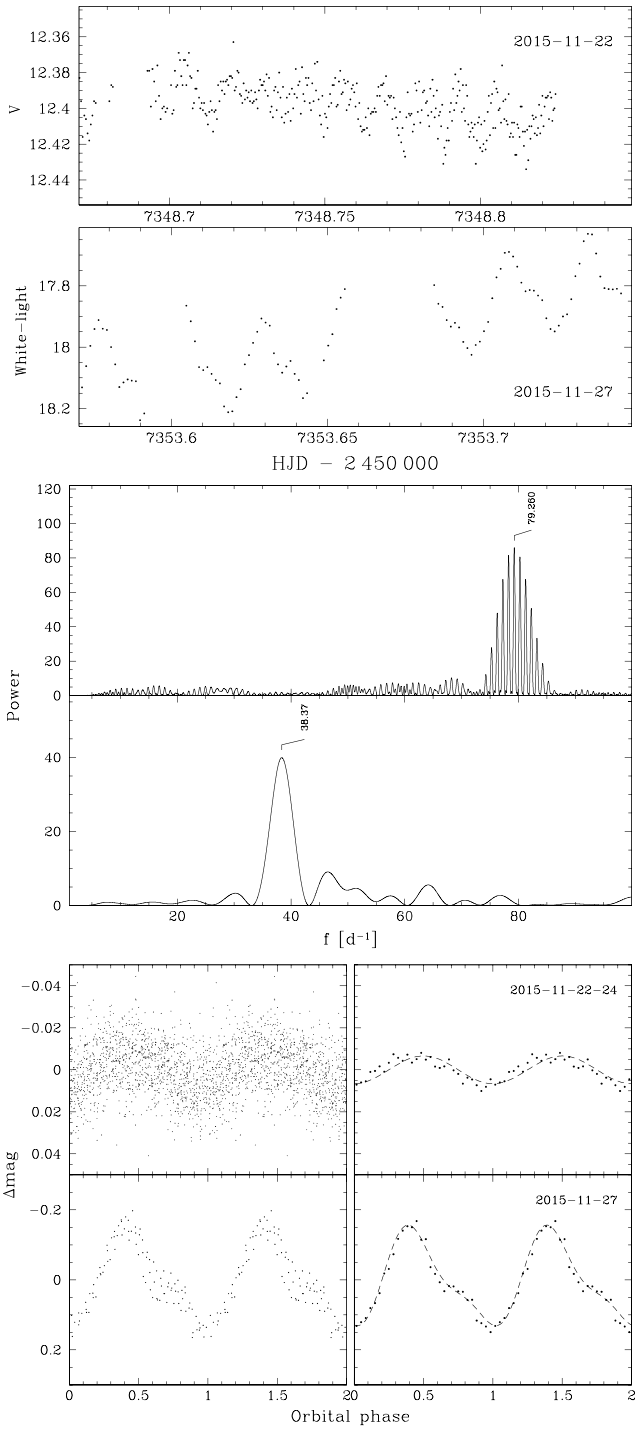

Figure 6. Top panels: The light curve of NSV1440 obtained on 2015 November 22 when the object was brightest exhibits clear short time-scale variations. By November 27, the object dropped in brightness by ~ 6 mag displaying larger-amplitude superhump structures in the light curve. Note that the scales on the horizontal axes are the same, so the periods of the variations are directly comparable. Middle panels: Scargle periodograms computed from the combined data obtained on 2015 November 22–24 (peak frequency $f = 79.260\,\mathrm{d}^{-1}$), and November 27 (peak frequency $f = 38.37\,\mathrm{d}^{-1}$). Bottom panels: The corresponding phase-folded light curves (left: individual observations; right: data binned into 30 phases) using the strongest signal detected in each of the two data sets. The superhump structure is clearly seen in the light curve.

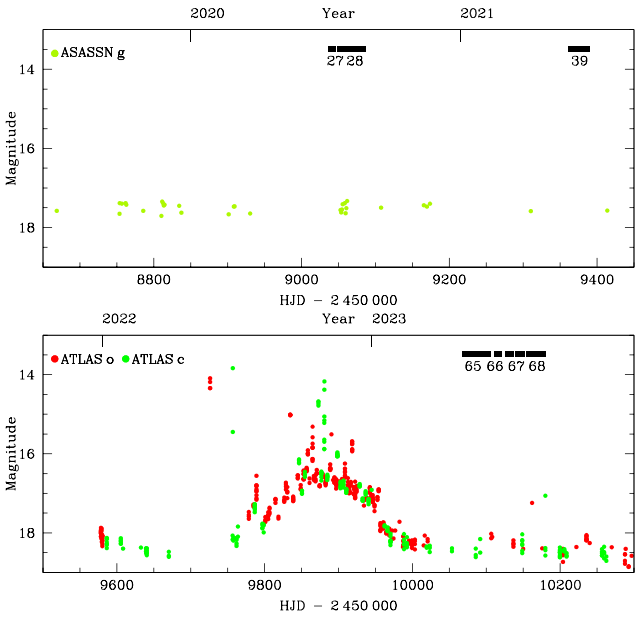

Figure 7. *TESS* observed NSV 1440 during quiescence in sectors 27, 28, and 39 (top panel, ASAS-SN *g*-band data in green). Late in 2022, the ATLAS cyan (*c*) and orange (*o*) bandpass light curves captured a bright state of NSV 1440 lasting $\simeq 200$ d. Throughout this high state, normal outbursts continued which indicates that the disc, or sufficiently large parts of it, were still undergoing thermal disc instabilities. *TESS* observed the system after its high state during sectors 65–68.

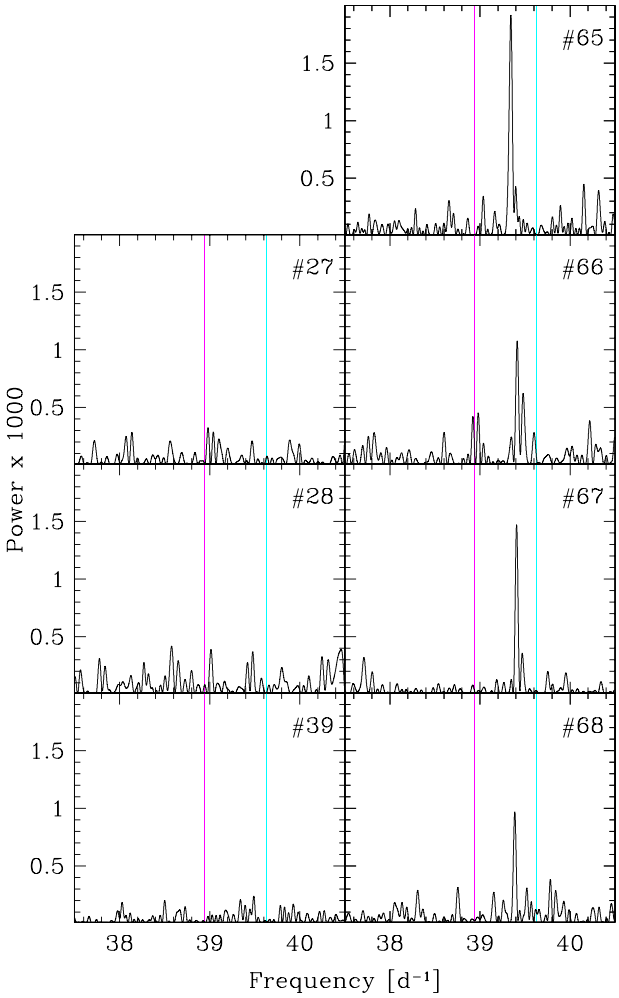

Figure 8. Power spectra computed from the seven sectors of *TESS* observations of NSV 1440. The magenta and cyan lines correspond to the early superhumps with $P = 36.335 \pm 0.071$ min) and the growing 'stage A' superhumps with $P = 36.978 \pm 0.029$ min of Isogai et al. (2019), who interpreted the early superhump signals as the orbital period. Each *TESS* light curve was normalized to a mean flux of unity prior to the analysis. Sectors 27, 28, and 39 were obtained in deep quiescence, and do not contain any significant signal. Sectors 65–68 were obtained $\simeq 100$–200 d after a 'high state' and independently show a strong signal at $\simeq 39.40\,\mathrm{d}^{-1}$, or $P = 36.56$ min. Given the stability of the period detected in the *TESS* data, we argue that this signal corresponds to the orbital period of NSV 1440.

We computed discrete Fourier transforms for all *TESS* observations (Fig. 8), finding no significant signal in the first three sectors, but detecting a strong signal at a mean value of 36.56 ± 0.03 min in the last four sectors. Given the stability of this period throughout nearly four months of *TESS* observations, we argue that this signal very likely represents the orbital period of the system, i.e. slightly longer than the value of 36.335 ± 0.071 min adopted by Isogai et al. (2019).

4.3 SDSS J1831+4202

We obtained time-series photometry of SDSS J1831+4202 during the period April 2023 to May 2024 for a total of 15 nights. The system was at a nearly constant brightness, 17.4–17.6 mag, except on 2023 April 28 when we found SDSS J1831+4202 in a fainter state at 18.5 mag. The system brightened again to 17.1 mag by the time of our next observation on 2023 May 3 (Table A4). Overall, the light curves obtained in the high state are characterized by short-time-scale variation of about 10–30 min with an amplitude of $\simeq 0.1$ mag. A clear superhump-like structure was detected in the 2023 May 3 light curve (Fig. 9, top panel). The periodogram of these data contains a strong peak at $f = 62.538 \pm 0.026\,\mathrm{d}^{-1}$ (Fig. 9, middle panel), or $P = 23.026 \pm 0.097$ min where the uncertainty was derived from a sine-fit to the data. The phase-folded light curve (Fig. 9, bottom panel) corroborates the superhump-like structure of the photometric variability. Our TNT observations confirm the period of 23.07374 ± 0.00001 min derived by Kato (2023) from the sparse ZTF data, and securely identify this photometric variability as either the orbital or a superhump signal. SDSS J1831+4202 was observed by *TESS* in Sectors 74, 80, and 81, but because of the contamination by a nearby bright star these data were not useful to refine the orbital period of the system.

5 DISCUSSION AND CONCLUSIONS

The formation and evolution of AM CVn stars are not well understood. There are three possible channels describing the formation of these binaries, characterized by the nature of the donor star. In the most compact binaries ($P_{\mathrm{orb}} < 10$ min) the primary white dwarf is thought to accrete materials from another white dwarf (Paczyński 1967), and in longer period systems from a partially degenerate He star (Savonije, de Kool & van den Heuvel 1986; Iben & Tutukov 1987). Some of the longest-period systems in the population may have formed as hydrogen CVs, but have lost their hydrogen

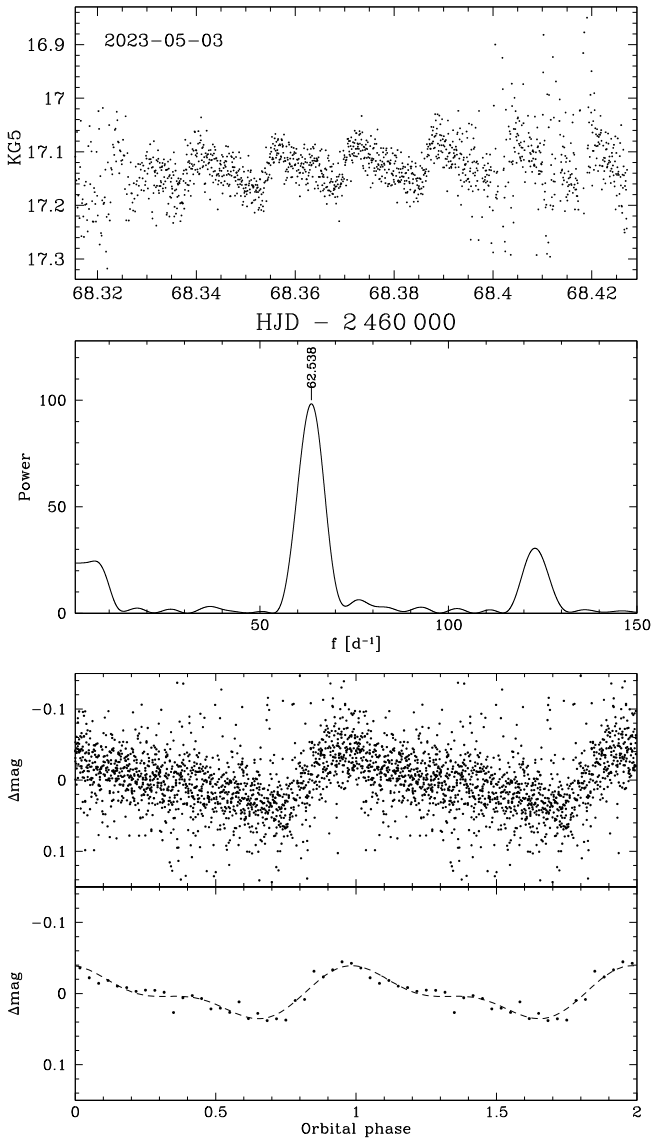

Figure 9. Top panel: The TNT light curve of SDSS J1831+4202 obtained on 2023 May 3 shows clear short-period variability. Middle panel: The Scargle periodogram of these data shows a strong peak at $f = 62.538\,\mathrm{d}^{-1}$. Bottom panels: The light curves (top: individual data; bottom: data binned into 30 phases) folded with $P = 23.026$ min.

envelopes through evolution and mass transfer (Podsiadlowski, Han & Rappaport 2003). One potential method to discriminate between the various evolutionary models is to assess the chemical composition of the donor star, set mainly by CNO-processing during the evolution (Nelemans et al. 2010). The amount of CNO-processing a helium star had undergone by the time it leaves the common envelope to become a mass-transferring AM CVn star determines the relative amounts of N and C left in the star, N/C > 100 for white dwarf donor models, but N/C < 10 for He star donors with $P_{\rm orb} > 20$ min (Nelemans et al. 2010). The most reliable way to measure the donor star abundances is by analysing the composition of the atmosphere of the primary, which is enriched with the accreted material (e.g. Toloza et al. 2019) – however, this requires in practically all cases high-quality ultraviolet spectroscopy. A less robust proxy for the composition of the donor is to investigate the relative strengths of the emission lines from the accretion flow (e.g. Gänsicke et al. 2003).

The spectrum of CRTS J0910−2008 is rich in neutral He, N, and Si, as well as ionized Ca and Fe. There is a slight redward asymmetry in the He I 5875 line, whose wavelength matches the Na I D doublet (e.g. Yamaguchi et al. 2023). Whereas our spectral range does not include any strong C lines, but the strength of the N lines, as well as the tentative detection of Na suggest that CRTS J0910−2008 is more likely to have a white dwarf donor than a helium star donor. No N is detected in the spectrum of NSV 1440, which could indicate a lower rate of conversion of C to N, and it is overall less metal-rich than that of CRTS J0910−2008, exhibiting only He, Si, and weak Ca lines.

Another method to constrain the donor parameters (and hence the evolutionary scenario) is through the superhump period excess (Green et al. 2018, 2020), if both the orbital and superhump periods are known.

Adopting the period measured from the long *TESS* observations as being the orbital period, $P_{\rm orb} = 36.56 \pm 0.03$ min, and the 'stage A' superhump period of Isogai et al. (2019), $P_{\rm sh} = 36.98$ min, we find a period excess of $\epsilon = (P_{\rm sh} - P_{\rm orb})/P_{\rm orb} = 0.011$, and a mass ratio of $q = M_2/M_1 = 0.032$, using equation (5) of Kato & Osaki (2013). Whereas this value is lower than that found by Isogai et al. (2019), it is still consistent with a semidegenerate donor.

The superhump period of CRTS J0910−2008 detected from the two outbursts in 2015 and 2018 is $P_{\rm sh} = 29.7$ min, but its orbital period is not yet known. Despite being fairly faint in quiescence, $G \simeq 19.4$, a spectroscopic determination of the orbital period is feasible thanks to the strong emission lines of this system. We confirm a photometric period of $P = 23$ min for SDSS J1831+4202, which may be either the orbital or (more likely) the superhump period. A spectroscopic measurement of $P_{\rm orb}$ will be challenging given the broad and shallow absorption lines in this system.

We show in Fig. 10 the location within the Hertzsprung–Russell diagram (HRD) of the 63 AM CVn stars that currently have both measured orbital or superhump periods as well as *Gaia* parallaxes (Green et al. 2024). As expected, SDSS J1831+4202 which spends most of the time in a high state with a hot and steady-state disc has the bluest $G_{\rm BP} - G_{\rm RP}$ colour. AM CVn stars with the longest orbital periods ($\gtrsim 50$ min) tend to cluster near, or within the white dwarf cooling sequence, reflecting the weak contribution of the accretion disc to the overall emission. Systems with frequent outbursts are distributed over a relatively large area of HRD parameter space, in fact, CRTS J0910−2008 is the reddest system in our study, even though it has a shorter period than NSV 1440. This somewhat scattered appearance in the HRD was discussed by Inight et al. (2022) as a consequence of *Gaia* sampling the systems at random epochs, resulting in average G, $G_{\rm BP}$, and $G_{\rm RP}$ magnitudes that do not necessarily reflect those of their most topical state. Hence, some care needs to be taken when predicting the properties of an AM CVn system solely based on its location in the HRD.

ACKNOWLEDGEMENTS

We thank the referee, Dr Oliveira Kepler, for a prompt and constructive report. This research has received funding support from the National Science, Research and Innovation Fund (NSRF) via the Program Management Unit for Human Resources & Institutional Development, Research and Innovation (grant no. B05F640046). This project has received funding from the European Research Council (ERC) under the European Union's Horizon 2020 research and innovation programme (grant agreement no. 101020057). This work has made use of data obtained at the Thai National Observatory

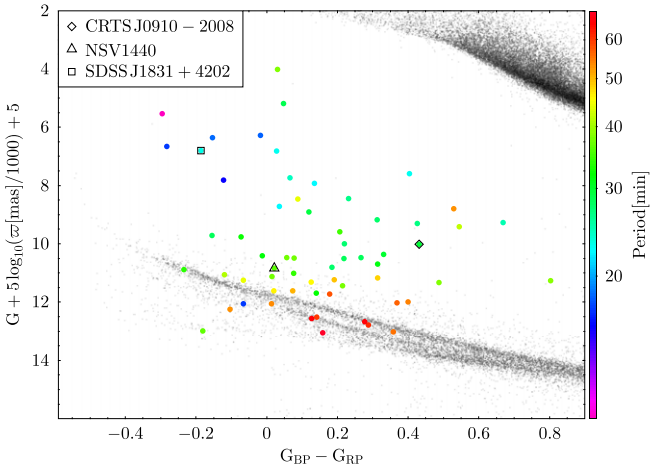

Figure 10. *Gaia* HRD displaying a selection of stars within 100 pc (grey) and the 63 confirmed AM CVn systems (coloured filled circles) with known orbital periods and *Gaia* parallaxes (from Green 2023). The newly confirmed systems are highlighted by black outlines SDSS J1831+4202 (square), NSV 1440 (triangle), and CRTS J0910−2008 (diamond). Systems with short orbital periods and high mass transfer rates tend to be intrinsically luminous and blue, in contrast, the systems with the longest orbital periods and lowest mass transfer rates are firmly located near or within the white dwarf cooling sequence. Systems undergoing dwarf nova outbursts show some scatter in the HRD, as the photometry within *Gaia* DR3 may have sampled different states (see the appendix of Inight et al. 2022).

on Doi Inthanon, operated by NARIT. This work has made use of data obtained by the PROMPT-8 telescope, owned by National Astronomical Research Institute of Thailand, and operated by the Skynet Robotic Telescope Network. The CSS survey is funded by the National Aeronautics and Space Administration under grant no. NNG05GF22G issued through the Science Mission Directorate Near-Earth Objects Observations Program. The CRTS survey is supported by the U.S. National Science Foundation under grants AST-0909182. This study is based on observations obtained with the Samuel Oschin 48-inch Telescope at the Palomar Observatory as part of the Zwicky Transient Facility project. ZTF was supported by the National Science Foundation under grant no. AST-1440341 and a collaboration including Caltech, IPAC, the Weizmann Institute for Science, the Oskar Klein Center at Stockholm University, the University of Maryland, the University of Washington, Deutsches Elektronen-Synchrotron and Humboldt University, Los Alamos National Laboratories, the TANGO Consortium of Taiwan, the University of Wisconsin at Milwaukee, and Lawrence Berkeley National Laboratories. Operations are conducted by COO, IPAC, and UW. This is also based on observations obtained at the Southern Astrophysical Research (SOAR) telescope, which is a joint project of the Ministério da Ciência, Tecnologia e Inovações (MCTI/LNA) do Brasil, the US National Science Foundation's NOIRLab, the University of North Carolina at Chapel Hill (UNC), and Michigan State University (MSU).

DATA AVAILABILITY

The ASAS-SN, ATLAS, and ZTF light curves can be retrieved from the respective archives, and we will make the TNT light curves available upon reasonable requests communicated to the lead author.

REFERENCES

Amaro-Seoane P. et al., 2012, Class. Quantum Gravity, 29, 124016
Bellm E. C. et al., 2019, PASP, 131, 018002
Bertin E., Arnouts S., 1996, A&AS, 117, 393
Bildsten L., Shen K. J., Weinberg N. N., Nelemans G., 2007, ApJ, 662, L95
Carter P. J. et al., 2013, MNRAS, 429, 2143
Clemens J. C., Crain J. A., Anderson R., 2004, in Moorwood A. F. M., Iye M., eds, Proc. SPIE Conf. Ser. Vol. 5492, Ground-Based Instrumentation for Astronomy. SPIE, Bellingham, p. 331
Currie M. J., Berry D. S., Jenness T., Gibb A. G., Bell G. S., Draper P. W., 2014, in Manset N., Forshay P., eds, ASP Conf. Ser. Vol. 485, Astronomical Data Analysis Software and Systems XXIII. Astron. Soc. Pac., San Francisco, p. 391
Dhillon V. S. et al., 2007, MNRAS, 378, 825
Dhillon V. S. et al., 2014, MNRAS, 444, 4009
Drake A. J. et al., 2009, ApJ, 696, 870
Duffy C. et al., 2021, MNRAS, 502, 4953
Gaia Collaboration, 2018, A&A, 616, A1
Gänsicke B. T. et al., 2003, ApJ, 594, 443
Green M., 2023, greenlabjhmi/rna_protein_crosslinks: v.10.23 (v.10.23), Zenodo. Available at: https://doi.org/10.5281/zenodo.8403056
Green M. J. et al., 2018, MNRAS, 477, 5646
Green M. J. et al., 2020, MNRAS, 496, 1243
Green M. J. et al., 2024, MNRAS, 527, 3445
Greenstein J. L., Matthews M. S., 1957, ApJ, 126, 14
Hardy L. K. et al., 2017, MNRAS, 465, 4968
Iben I., Jr, Tutukov A. V., 1987, ApJ, 313, 727
Inight K. et al., 2022, MNRAS, 510, 3605
Inight K. et al., 2023, MNRAS, 524, 4867
Isogai K., Kato T., Monard B., Hambsch F.-J., Myers G., Starr P., Cook L. M., Nogami D., 2019, PASJ, 71, 48
Kato T., 2015, PASJ, 67, 108
Kato T., 2023, preprint (arXiv:2307.08954)
Kato T., Osaki Y., 2013, PASJ, 65, 97
Kato T., Stubbings R., 2023, preprint (arXiv:2305.04194)
Kato M., Hachisu I., Kiyota S., Saio H., 2008, ApJ, 684, 1366
Kato T. et al., 2009, PASJ, 61, 395
Khalil J. M. et al., 2024, A&A, 683, L10
Kochanek C. S. et al., 2017, PASP, 129, 104502
Korol V., Rossi E. M., Groot P. J., Nelemans G., Toonen S., Brown A. G. A., 2017, MNRAS, 470, 1894
Kotko I., Lasota J.-P., Dubus G., Hameury J.-M., 2012, A&A, 544, A13
Kupfer T. et al., 2018, MNRAS, 480, 302
Levitan D. et al., 2011, ApJ, 739, 68
Levitan D., Groot P. J., Prince T. A., Kulkarni S. R., Laher R., Ofek E. O., Sesar B., Surace J., 2015, MNRAS, 446, 391
Marsh T. R., 1989, PASP, 101, 1032
Marsh T. R., Nelemans G., Steeghs D., 2004, MNRAS, 350, 113
Masci F. J. et al., 2019, PASP, 131, 018003
Nelemans G., Yungelson L. R., Portegies Zwart S. F., 2004, MNRAS, 349, 181
Nelemans G., Yungelson L. R., van der Sluys M. V., Tout C. A., 2010, MNRAS, 401, 1347
Osaki Y., 1974, PASJ, 26, 429
Paczyński B., 1967, Acta Astron., 17, 287
Patterson J. et al., 2005, PASP, 117, 1204
Podsiadlowski P., Han Z., Rappaport S., 2003, MNRAS, 340, 1214
Ramsay G., Barclay T., Steeghs D., Wheatley P. J., Hakala P., Kotko I., Rosen S., 2012, MNRAS, 419, 2836
Ramsay G. et al., 2018, A&A, 620, A141
Rivera Sandoval L. E., Maccarone T. J., Pichardo Marcano M., 2020, ApJ, 900, L37
Rivera Sandoval L. E., Maccarone T. J., Cavecchi Y., Britt C., Zurek D., 2021, MNRAS, 505, 215
Rivera Sandoval L. E., Heinke C. O., Hameury J. M., Cavecchi Y., Vanmunster T., Tordai T., Romanov F. D., 2022, ApJ, 926, 10
Rodriguez A. C. et al., 2023, ApJ, 954, 63

Savonije G. J., de Kool M., van den Heuvel E. P. J., 1986, A&A, 155, 51
Scargle J. D., 1982, ApJ, 263, 835
Shappee B. J. et al., 2014, ApJ, 788, 48
Shen K. J., Bildsten L., 2014, ApJ, 785, 61
Smak J., 1967, Acta Astron., 17, 255
Solheim J., 2010, PASP, 122, 1133
Steeghs D. et al., 2022, MNRAS, 511, 2405
Toloza O. et al., 2019, Bulletin of the American Astronomical Society, Vol. 51, Astro2020: Decadal Survey on Astronomy and Astrophysics. p. 168
van Roestel J. et al., 2021, AJ, 162, 113
van Roestel J. et al., 2022, MNRAS, 512, 5440
Watson C. L., Henden A. A., Price A., 2006, Soc. Astron. Sci. Annu. Symp., 25, 47
Whitehurst R., King A., 1991, MNRAS, 249, 25
Woudt P. A. et al., 2009, ApJ, 706, 738
Yamaguchi N., El-Badry K., Rodriguez A. C., Gull M., Roulston B. R., Vanderbosch Z. P., 2023, MNRAS, 524, 740

APPENDIX: OBSERVATION LOGS

Table A1. Comparison stars used for the differential photometry.

Comparison star	Identifier	Magnitudes
C1	USNO-A2.0 0675-10057431	$B = 15.5$, $R = 15.0$
C2	USNO-A2.0 0675-10058614	$B = 17.8$, $R = 17.0$
C3	USNO-A2.0 0675-10058349	$B = 13.5$, $R = 13.7$
C4	USNO-A2.0 0675-10062884	$B = 13.9$, $R = 14.0$
C5	USNO-A2.0 0675-10058295	$B = 16.6$, $R = 16.0$
C6	USNO-A2.0 0075-00639610	$B = 12.7$, $R = 12.1$
C7	USNO-A2.0 0075-00642821	$B = 15.3$, $R = 16.5$
C8	USNO-A2.0 0075-00643994	$B = 13.9$, $R = 16.0$
C9	USNO-A2.0 1275-10094237	$B = 16.2$, $R = 15.2$

Table A2. Log of the photometric observations of CRTS J0910−2008.

Date	UT	Telescope	Filter	Exp. (s)	Frames	Comparison star	Mag.
2015 Feb 12	03:46-07:59	PROMPT8	*V*	30	208	C1	16.4
2015 Feb 13	01:13-08:55	PROMPT8	*V*	45	286	C1	15.9
2015 Feb 14	01:04-08:56	PROMPT8	*V*	35	355	C1	16.6
2015 Feb 15	01:05-07:16	PROMPT8	*V*	55	149	C1	17.5
2015 Feb 16	02:01-07:59	PROMPT8	*V*	40	217	C1	16.8
2015 Feb 17	00:33-07:59	PROMPT8	*V*	100	135	C1	18.1
2015 Feb 19	00:22-09:08	PROMPT8	*V*	100	69	C1	18.6
2015 Feb 22	00:19-08:43	PROMPT8	*V*	100	64	C1	18.8
2015 Feb 23	00:18-08:54	PROMPT8	*V*	100	61	C1	18.9
2015 Feb 24	00:17-08:38	PROMPT8	*V*	100	58	C1	19.0
2015 Feb 25	00:16-08:19	PROMPT8	*V*	100	33	C1	19.1
2015 Feb 26	00:14-08:27	PROMPT8	*V*	100	37	C1	19.1
2015 Feb 27	00:13-00:22	PROMPT8	*V*	100	5	C1	>19.1
2018 Jan 14	16:24-17:39	TNT	*KG5*	30	135	C2	20.3
2018 Feb 22	16:50-18:56	TNT	*KG5*	30	221	C2	20.4
2018 Feb 24	14:47-14:49	TNT	*KG5*	30	4	C2	19.9
2018 Mar 03	14:05-14:05	TNT	*KG5*	30	2	C2	19.1
2018 Mar 04	12:33-12:36	TNT	*KG5*	5, 30	13	C2	19.0
2018 Mar 05	14:55-14:56	TNT	*KG5*	30	3	C2	19.6
2018 Mar 18	12:27-18:01	TNT	*KG5*	1	6431	C3	14.0
2018 Mar 19	12:24-18:16	TNT	*KG5*	3	4530	C3	14.2
2018 Mar 20	12:20-18:18	TNT	*KG5*	3	5157	C3	14.3
2018 Mar 22	15:47-17:59	0.5 m-TNO	*V*	20	352	C3	14.8
2018 Mar 23	14:07-17:45	0.5 m-TNO	*V*	20	563	C3	14.9
2018 Mar 24	14:42-17:46	0.5 m-TNO	*V*	20	188	C3	15.8
2018 Mar 27	12:38-13:19	0.5 m-TNO	*V*	120	19	C3	16.8
2018 Mar 28	01:02-03:20	ROAD 0.4 m	*CV*	60	82	C4	15.9
2018 Mar 30	02:16-04:22	ROAD 0.4 m	*CV*	60	48	C4	17.3
2018 Mar 31	03:57-04:19	ROAD 0.4 m	*CV*	60	10	C4	16.7
2018 Apr 01	03:53-04:15	ROAD 0.4 m	*CV*	60	10	C4	16.4
2018 Apr 03	00:31-04:07	ROAD 0.4 m	*CV*	60	98	C4	17.5
2018 Apr 04	03:40-04:03	ROAD 0.4 m	*CV*	60	9	C4	16.3
2018 Apr 05	03:37-03:57	ROAD 0.4 m	*CV*	60	8	C4	18.0
2018 Apr 06	03:33-03:53	ROAD 0.4 m	*CV*	60	8	C4	17.9
2018 Apr 06	12:45-14:50	TNT	*KG5*	15	432	C5	17.9
2018 Apr 07	03:29-03:49	ROAD 0.4 m	*CV*	60	8	C4	18.4
2018 Apr 08	03:22-03:44	ROAD 0.4 m	*CV*	60	9	C4	18.4
2018 Apr 08	12:32-15:55	TNT	*KG5*	15	773	C5	18.0
2018 Apr 09	03:21-03:41	ROAD 0.4 m	*CV*	60	8	C4	18.5
2018 Apr 10	03:22-03:37	ROAD 0.4 m	*CV*	60	4	C4	18.6
2021 Apr 01	14:38-14:39	TNT	*KG5*	15	5	C5	19.4
2021 Apr 02	13:46-13:54	TNT	*KG5*	15, 30	13	C5	19.8
2023 Jan 22	19:03-19:26	TNT	*KG5*	15	76	C5	19.2
2023 Mar 10	12:36-12:42	TNT	*KG5*	30	13	C5	19.0
2023 Mar 11	16:38-16:41	TNT	*KG5*	15	10	C5	19.1
2023 Mar 17	13:06-13:08	TNT	*KG5*	15	10	C5	18.9
2023 Apr 10	14:35-14:38	TNT	*KG5*	15	10	C2	19.4
2023 Apr 17	14:22-14:25	TNT	*KG5*	15	10	C2	19.4
2023 Apr 23	14:07-14:09	TNT	*KG5*	15	5	C2	19.1
2023 Apr 24	14:04-14:07	TNT	*KG5*	15	10	C2	19.3
2023 Apr 28	14:13-14:17	TNT	*KG5*	15	6	C2	18.7
2024 Feb 22	17:17-17:20	TNT	*KG5*	10	15	C5	19.0

Table A3. Log of the photometric observations of NSV 1440.

Date	UT	Telescope	Filter	Exp. (s)	Frames	Comparison star	Mag.
2015 Nov 22	04:06-07:49	PROMPT8	*V*	20	350	C6	12.4
2015 Nov 23	04:34-07:45	PROMPT8	*V*	10	452	C6	12.5
2015 Nov 24	05:00-07:41	PROMPT8	*V*	10	381	C6	12.6
2015 Nov 26	05:56-06:49	PROMPT8	Clear	100	20	C7	18.7
2015 Nov 27	01:41-05:53	PROMPT8	Clear	100	100	C7	17.9
Long time series:							
	No. of nights						Mag range
2015 Nov 21 to 2016 Jan 9	50	ROAD 0.4 m	*CV*	30–60	3894	C8	12.96–18.13
2019 Feb 17 to 2019 Apr 25	68	ROAD 0.4 m	*CV*	30	2363	C8	13.44–18.04
TESS:							
	Sector						
2020 Jul 05 to 2020 Jul 28	27	*TESS*	*T*	120	13490		
2020 Jul 31 to 2020 Aug 24	28	*TESS*	*T*	120	14909		
2021 May 27 to 2021 Jun 24	39	*TESS*	*T*	120	19377		
2023 May 05 to 2023 Jun 01	65	*TESS*	*T*	120	18968		
2023 Jun 02 to 2023 Jun 25	66	*TESS*	*T*	120	11777		
2023 Jul 01 to 2023 Jul 25	67	*TESS*	*T*	120	13661		
2023 Jul 29 to 2023 Aug 22	68	*TESS*	*T*	120	15334		

Table A4. Log of the photometric observations of SDSS J183131.63+420220.2.

Date	UT	Telescope	Filter	Exp. (s)	Frames	Comparison star	Mag.
2023 Apr 10	18:44-22:34	TNT	*KG5*	10	1223	C9	17.4
2023 Apr 24	21:02-22:17	TNT	*KG5*	5	752	C9	17.8
2023 Apr 28	17:12-19:57	TNT	*KG5*	10	874	C9	18.5
2023 May 03	19:34-22:15	TNT	*KG5*	5	1439	C9	17.1
2023 May 04	20:47-21:42	TNT	*KG5*	5	366	C9	17.2
2024 Mar 30	21:54-22:39	TNT	*KG5*	10	246	C9	17.4
2024 Apr 01	21:49-22:41	TNT	*KG5*	5	528	C9	17.4
2024 Apr 17	19:54-22:20	TNT	*KG5*	8	969	C9	17.4
2024 Apr 23	16:41-22:11	TNT	*KG5*	5	1457	C9	17.4
2024 Apr 25	19:11-22:14	TNT	*KG5*	5	1232	C9	17.4
2024 Apr 27	19:23-19:47	TNT	*KG5*	5	65	C9	17.5
2024 Apr 29	19:23-22:12	TNT	*KG5*	10	774	C9	17.5
2024 May 06	18:00-18:24	TNT	*KG5*	7	183	C9	17.6
2024 May 07	18:30-18:56	TNT	*KG5*	7	175	C9	17.4
2024 May 12	17:52-19:28	TNT	KG5	5	939	C9	17.4

Table A5. Photometric periods detected in the three AM CVn stars.

Object	Date	*P* (min)
CRTS J0910−2008	2015 Feb 12–16	29.677 ± 0.004
	2018 Mar 18–19	30.073 ± 0.009
	2018 Mar 20 Mar	30.199 ± 0.016
	2018 Mar 22–23	29.722 ± 0.007
	2015 Feb 12–16 + 2018 Mar 22–23	29.700 ± 0.004
NSV1440	2015 Nov 22–24	37.53 ± 0.13
	2019 Feb 17–20	36.525 ± 0.017
	2023 May 05 to Jun 01	36.6019 ± 0.0019
	2023 Jun 02 to Jun 25	36.5361 ± 0.0037
	2023 Jul 01 to Jul 25	36.5419 ± 0.0020
	2023 Jul 29 to Aug 22	36.5599 ± 0.0027
SDSS J183131.63+420220.2	2023 May 03	23.026 ± 0.097

This paper has been typeset from a TEX/LATEX file prepared by the author.